Splitting of a Vertical Multiwalled Carbon Nanotube Carpet to a Graphene Nanoribbon Carpet and Its Use in Supercapacitors

ARTICLE *in* ACS NANO · MAY 2013

Impact Factor: 12.88 · DOI: 10.1021/nn400750n · Source: PubMed

9 AUTHORS, INCLUDING:

Zhiwei Peng
University of Maryland, College Park
49 PUBLICATIONS **1,483** CITATIONS
SEE PROFILE

Jian Lin
University of Missouri
42 PUBLICATIONS **995** CITATIONS
SEE PROFILE

Chih-Chau Hwang
Rice University
17 PUBLICATIONS **317** CITATIONS
SEE PROFILE

Wei Lu
Weatherford International
37 PUBLICATIONS **2,635** CITATIONS
SEE PROFILE

Splitting of a Vertical Multiwalled Carbon Nanotube Carpet to a Graphene Nanoribbon Carpet and Its Use in Supercapacitors

Chenguang Zhang,[†,‡,§,#] Zhiwei Peng,[†,#] Jian Lin,[‡,⊥] Yu Zhu,[†,‡] Gedeng Ruan,[†] Chih-Chau Hwang,[†] Wei Lu,[†] Robert H. Hauge,[†,‡,*] and James M. Tour[†,‡,⊥,∥,*]

[†]Department of Chemistry, [‡]Smalley Institute for Nanoscale Science and Technology, Rice University, Houston, Texas 77005, United States, [§]School of Materials Science and Engineering, Tianjin University, No. 92 Weijin Road, Tianjin, China 300072, and [⊥]Department of Mechanical Engineering and Material Science and [∥]Department of Computer Science, Rice University, 6100 Main Street, Houston, Texas 77005, United States. [#]These authors contributed equally to this work.

ABSTRACT

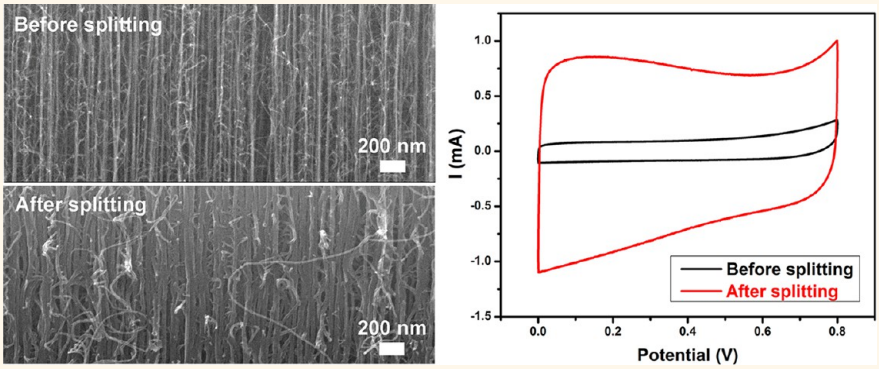

Potassium vapor was used to longitudinally split vertically aligned multiwalled carbon nanotubes carpets (VA-CNTs). The resulting structures have a carpet of partially split MWCNTs and graphene nanoribbons (GNRs). The split structures were characterized by scanning electron microscopy, transmission electron microscopy, atomic force microscopy, Raman spectroscopy and X-ray photoelectron spectroscopy. When compared to the original VA-CNTs carpet, the split VA-CNTs carpet has enhanced electrochemical performance with better specific capacitance in a supercapacitor. Furthermore, the split VA-CNTs carpet has excellent cyclability as a supercapacitor electrode material. There is a measured maximum power density of 103 kW/kg at an energy density of 5.2 Wh/kg and a maximum energy density of 9.4 Wh/kg. The superior electrochemical performances of the split VA-CNTs can be attributed to the increased surface area for ion accessibility after splitting, and the lasting conductivity of the structure with their vertical conductive paths based on the preserved GNR alignment.

KEYWORDS: vertically aligned multiwalled carbon nanotubes · split VA-CNTs · graphene nanoribbon carpets · supercapacitor · specific capacitance · energy density · power density

Carbon nanotubes (CNTs) are materials that are desirable to integrate into many applications due to their high mechanical strength, high electrical and thermal conductivity as well as reasonable specific surface area.[1] Graphene nanoribbons (GNRs) can be formed from the tubular CNT structures through longitudinal splitting and flattening. In this way, the dimensions of the GNRs can be predetermined by the initial CNT length and diameter. While there are lithographic[2] and chemical methods[3] for making GNRs, the reductive splitting techniques hold the potential for consistent production of GNRs. Splitting methods include partial etching with Ar plasma,[4] Li atom intercalation,[5] abrupt thermal expansion,[6] nanoparticle cutting[7] and electrical unwrapping of MWCNTs.[8] A recent study by Dai[9] realized a partial splitting of few-walled nanotubes, which exhibit catalytic activity for oxygen reduction.

* Address correspondence to hauge@rice.edu, tour@rice.edu.

Received for review February 13, 2013 and accepted May 14, 2013.

Published online May 14, 2013
10.1021/nn400750n

A potentially scalable technique for making graphene oxide nanoribbons from longitudinal splitting of MWCNTs through chemical oxidation is available.[10] MWCNTs can also be reductively split using potassium vapor[11] or liquid Na/K alloy,[12−14] an advantage because the split product is free of oxidative defects and *in situ* functionalization can be done. To date, the nanotube materials for bulk-scale unzipping or splitting are usually in a randomly dispersed solid powder or colloidal suspension form. A few studies have been done on the splitting behavior of a predefined nanotube array in a nanotube electronic device[15] or horizontally aligned arrangement.[16] An important highly ordered assembled form of CNTs is a carpet vertically grown on a substrate. The vertically aligned CNTs (VA-CNTs) offer high surface area, simple growth by a well-developed chemical vapor deposition method and good structural control by adjustment of the growth parameters. Therefore, VA-CNTs are potential candidates for energy storage electrodes,[17] field emitters[18] and transparent films.[19] Recently, the splitting of aligned MWCNT sheets has been applied to GNR yarn spinning.[20] However, there are no other reports of the unzipping or splitting of VA-CNT arrays. Splitting the VA-CNTs while maintaining the vertically integrity of the VA-CNT starting material should further increase the accessible surface area, thus facilitating various device fabrications.

As energy storage materials, a supercapacitor is known for its high-power density and long-cycled lifetime,[21] desirable characteristics in automotive and portable energy-storage media that complement batteries and regenerative energy applications.[22] CNTs are candidates for the electrodes in supercapacitors due to their high surface area, excellent conductivity and chemical inertness. For making electrochemical supercapacitors, the VA-CNT array appears to be advantageous over both randomly deposited CNT networks[23] and the commercially used activated carbon capacitors, in terms of its regular pore structure and straight conductive paths that can provide good ion accessibility, fast ion diffusion and high rate-tolerant capacitance.[24] VA-CNT carpets have been grown on conductive substrates[24−28] or transferred onto metallic substrates[29−31] to be employed in carbon-based supercapacitors. In comparison to batteries, the major drawback of the supercapacitors is the relatively low energy densities. The maximum storage energy is given by $CV^2/2$, where C is the capacitance and V is the potential window. One strategy to enhance the energy density is through enlarging the operating voltage range by using an organic-based electrolyte.[32] The VA-CNT carpet provides another possible route to boost the energy density by increasing the capacitance.

Here, we demonstrate the splitting of VA-CNTs with preservation of vertical integrity to produce a mixture of split MWCNTs and GNRs. Potassium vapor intercalation and subsequent solvent quenching produced the split VA-CNTs. Partially split regions were formed due to the reaction of the outer MWCNT layers while the inner few-walled nanotubes did not react. The work here combines the concept of splitting the VA-CNT carpet with an improvement in ion accessibility due to the opening of the side-walls. The largely opened spaces and the aligned vertical structure can not only increase the effective surface area for the ions, but also provides easily accessible paths for fast ion transport. The intact inner few-walled nanotubes serve as conductors for charge transport. These advantages lead to the better electrochemical performance of split VA-CNT carpets when compared to the as-prepared VA-CNT in terms of the supercapacitor specific capacitance and power density. In addition, the free-standing split VA-CNT carpet was used in dual functions, as both an electrode and a current collector, thus avoiding the need for another metallic current collector. This simplifies the device fabrication process and makes the split VA-CNTs candidates for use in lightweight energy storage devices.

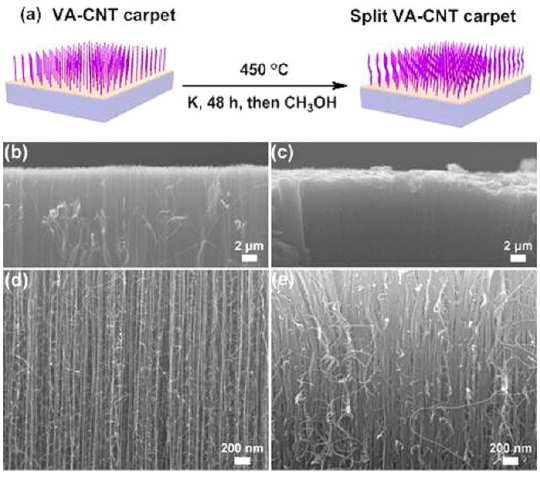

Figure 1. Process for splitting a VA-CNT carpet and SEM characterization. (a) Schematic illustration of splitting VA-CNT carpet by potassium atom intercalation and subsequent splitting. The middle layer in light pink represents the Al_2O_3 and Fe film, and the bottom layer in light gray represents the SiO_2 substrate. (b and c) SEM images of the VA-CNT carpets before and after splitting, respectively, at low magnification. (d and e) SEM images of the VA-CNT carpets before and after splitting, respectively, at higher magnification.

RESULTS AND DISCUSSION

Figure 1a is a scheme of the VA-CNT carpet splitting process, during which the potassium vapor intercalation reaction is conducted for 48 h at 450 °C. After the reaction, ethyl ether was added to cover the product, followed by the addition of methanol to quench the reaction. Scanning electron microscopy (SEM) images of the VA-CNT carpet before and after splitting are shown in Figure 1b−e. Figure 1b,c shows that the vertically aligned structure was preserved after splitting. Figure 1d shows that in the as-grown VA-CNT

carpet, the individual nanotubes were densely packed and vertically aligned. There are few disordered bundles contained in the as-grown sample. Moreover, the MWCNTs were quite straight with aligned pores, a property that could be beneficial for the introduction and transport of electrolyte ions when compared to the tortuous pore structure in activated carbon.[33] After splitting, as shown in Figure 1e, the nanotubes become flattened along their entire length and the widths have widened due to the transformation from CNTs to partially split CNTs and GNRs. The magnified SEM images that confirm the split structures are shown in Figure S1a,b. The vast majority of the split CNTs maintain their vertical alignment, and the aligned spaces among the CNTs are narrowed due to partial splitting or complete GNR formation. Some of the small-diameter CNTs that lost alignment are still intact and kept their cylindrical shape. The preservation of the vertical integrity of the split CNTs and GNRs can be attributed to the strong van der Waals interactions among the nanostructures. However, careful handling of the split sample was required during the washing procedure (Methods). To maintain the vertical structure of the product, the split VA-CNTs were not treated with sonication in chlorosulfonic acid, in contrast to prior work.[11]

Transmission electron microscopy (TEM) images of individual MWCNTs from VA-CNTs before and after splitting are shown in Figure 2. Figure 2a shows an individual MWCNT before splitting which has a hollow and cylindrical inner canal with typically 8−10 walls and an average width of ∼10 nm. After splitting, the widths of the resulting GNRs became larger, > 20 nm (Figure 2b−d). As can be seen in Figure 2b,c, partial splitting occurred on the outer walls, forming GNRs outside the intact inner tubes, of which about 4−5 walls remain. The partial splitting may be due to the higher crystallinity of the inner walls when compared to the outer walls. Therefore, potassium atoms may only insert into the interstitial spaces of the outermost walls of the MWCNTs. Solvation of potassium ions and the hydrogen gas evolution induced by the methanol quenching could then initiate the exfoliation around the intercalated potassium and the splitting would propagate longitudinally.[11] The outer GNRs formed a uniform coating on the outside of the inner tubes (Figure S1c). However, the crystalline structure could be destroyed in part by quenching;[34] therefore, after deintercalation and splitting, the outer graphitic layer can form short-range disordered graphene layers (Figure 2b,c and Figure S1d). The occasionaly observed partial separation of the inner tubes (Figure 2c and S1d) could be attributed to the vigorous bath sonication treatment during the TEM sample preparation. The inner tubes are unlikely split under these conditions,[9] probably due to the high graphitic crystallinity of the inner few-walled nanotubes (single-walled, double-walled or triple-walled nanotubes), although single-walled carbon nanotubes (SWCNTs) can react with potassium under some circumstances.[35,36] Splitting over the entire length can also be observed, portions of which are shown in Figure 2d and Figure S1e, which show that the herringbone-like graphitic walls are formed *via* splitting the straight walls of the original tube along its long axis. Therefore, we can observe that some nanotubes are GNR-wrapped, along with incomplete nanotrough-like split lines along their longitudinal directions (Figure S1a). There may not be enough driving force for the tips of the cleft to expand due to the large van der Waals interaction between the side-walls and the intrinsic curling structure of the nanotubes. Also, the deintercalation of the metal atoms could result in slowing and prevention of the splitting.[37]

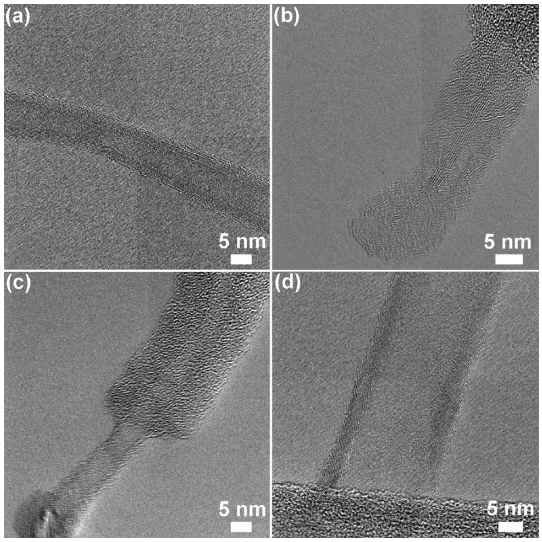

Figure 2. TEM characterizations of nanotubes from the VA-CNT carpet before and after splitting. (a) TEM image of an as-prepared MWCNT from a VA-CNT carpet. (b−d) TEM images of MWCNTs from a VA-CNT array after splitting. (b and c) The partial splitting in which the GNRs formed by the splitting are outside the inner intact tubes. (d) A MWCNT entirely split into a layer of GNRs exhibiting a herringbone-like edge structure when viewed by TEM.[11]

Water etching is usually employed to remove the amorphous carbon that is attached to the outermost wall of a nanotube.[19] Therefore, the split VA-CNT carpet was subjected to high-temperature water etching at 900 °C for 0.5 h. Figure S1f shows that the uniform coatings on the outer walls are intact, indicating they are formed by reaction between the outer MWCNT layers and potassium vapor followed by splitting instead of being amorphous carbon that was physisorbed during the VA-CNT growth process.

Atomic force microscopy (AFM) (Figure 3) characterization was also carried out to demonstrate the structural change after splitting the VA-CNTs. The AFM samples were bath sonicated to form a dispersed solution, followed by spin-coating the sample on top

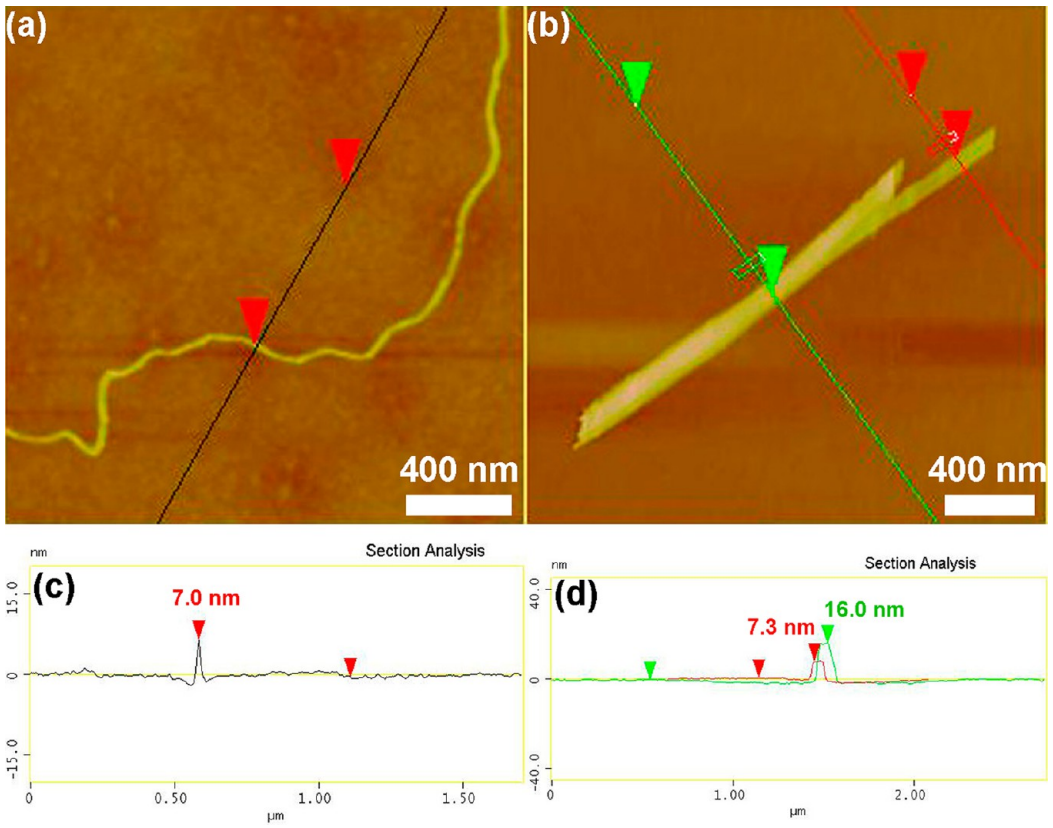

Figure 3. AFM characterization of an individual nanostructure from the VA-CNT carpet before and after splitting. (a and b) Tapping mode AFM height images of MWCNTs before and after splitting, respectively. (c and d) Height measurement profiles corresponded to the red and green triangle markers on the crossing lines in (a) and (b). The different heights measured from two different sections in (b) suggest the stacking of two superimposed split ribbon stacks.

of the SiO_2 wafer. Figure 3a,c indicates that the nanotube has a height measurement of ~7 nm, which is the typical height for these MWCNTs, consistent with the diameter measurement from TEM. Figure 3b shows a ribbon-like structure with several layers on a partially stacked assembly with increased width. This indicates that even though the tube walls have been fully split into GNRs, the strong van der Waals interaction keeps them from exfoliating during the sample preparation (Figure S2). In another region, an extracted split inner tube can be observed in the AFM image (Figure S3a,b). Interestingly, a splitting line is clearly observed on top of the nanotube, as indicated in the three-dimensional AFM image (Figure S3c), in analogy to the longitudinal splitting of a rubber hose that does not entirely flatten.

Figure 4 shows the Raman and X-ray photoelectron spectroscopy (XPS) spectra that were obtained to further show the structural changes after splitting. As shown in Figure 4a, there is little change in the G/D ratio, which is related to the structural continuity of the nanotubes, indicating that the splitting process introduces little damage to the nanotube quality apart from the split. The disordered structure caused by the splitting and exfoliation is shown by the broadening of the G and 2D band as well as the combination mode D+G band in the Raman spectra of the split sample.[11,38] Compared to the previous study,[11] higher temperature (450 °C) and longer duration (48 h) for intercalation of potassium were used in this work. This resulted in more disordered structures of the split sample than the split MWCNT made in the previous work, which were treated at 250−350 °C and for 14 h.[11] As can be seen in Figure 4b, the lack of K signal in the XPS spectra of the split product indicates that the oxygen did not come from residual methoxide.[37] The slight increase in oxygen signal after the splitting can be attributed to physisorbed oxygen. Furthermore, the absence of signals at 286 and 287 eV, corresponding to C−O and C═O (Figure S4), further confirm that no oxidation occurred during the splitting process.

To demonstrate the advantages of the split VA-CNT carpet over unsplit VA-CNTs in terms of potential applications, the electrochemical supercapacitor performance of the unsplit and split VA-CNTs were compared. Figure S5a is the scheme of the fabricated supercapacitor device using the VA-CNT or split VA-CNT carpet. A free-standing split VA-CNT carpet film after wet-etching the substrate is also shown in the image. The area of the free-standing VA-CNT carpet film electrode is 0.2 cm^2. Both of the VA-CNT films before and after splitting maintain their complete structure and can be easily handled by tweezers,

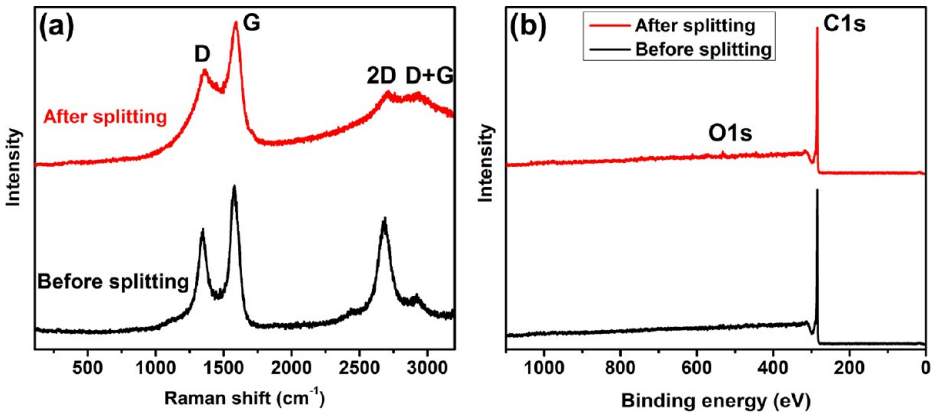

Figure 4. Raman and XPS characterization. (a) Raman spectra of the VA-CNT carpets before and after splitting. (b) XPS spectra of the VA-CNT carpets before and after splitting.

facilitating their transfer onto the backing plate of the supercapacitor device. The CNT film was used as both the electrode material and the current collector. The CNT films were assembled onto the separator with the electrolyte solution and then sandwiched by the two stainless steel backing plates to complete the assembly of the system.[39,40] Unlike the direct employment of metallic substrates for growing the current collector, we obtained the free-standing VA-CNT carpet by dissolving the substrate from the carpet using acid. This avoids a potential problem of the substrate suffering from instability in the electrolyte environment during long-term cycling. By using the free-standing VA-CNT carpet as both the electrode and current collector, the device fabrication process was simplified. It is reported that avoiding the use of the metallic current collector will increase the potential distribution across the thickness direction of the CNT electrode, thus lowering the capacitance.[31] However, the lack of an extra current collector can maximize the overall energy and power density.

Cyclic voltammetry (CV) at a scanning rate of 0.1 V/s and an operation voltage window of 0.8 V was used to test the VA-CNTs. As seen in Figure 5a, the split VA-CNT carpet shows greatly enhanced electrochemical performance compared to that of the sample without splitting. The power density of the split VA-CNT carpet, which is indicated by the integrated area, is much larger than that of the as-prepared VA-CNT electrode. The CV curve shows the fast current response to the change in voltage sweep direction, and the shape is near-rectangular until 1 V/s (Figure S5), indicating the formation of an electrochemical double layer. The electrochemical properties were stable during a number of CV cycles, which indicates a stable delivery of ions and good connections between the CNT electrode and the current collector. The superior capacitance behavior and power density of the split VA-CNT carpet is also demonstrated by the analyses at scanning rates of 0.5 and 1 V/s (Figure S5b-c). The specific capacitances, derived from galvanostatic charge–discharge curves with different current densities, of the VA-CNT carpet before and after splitting are shown in Figure S6a. Compared to the original VA-CNT carpet, the splitting increased the specific capacitance by ~4 times (106.2 F/g) at a small discharge current density, and outperforms the original VA-CNT carpet by ~3 times at high discharge current density. The specific capacitance of the split VA-CNT carpet is much higher than in previous studies using the VA-CNT as electrode material,[26−29,31] and are comparable to that of oxidized VA-CNT in ionic liquid and organic electrolyte.[24] The capacitance improvement can be attributed to the combination of a more effective surface area for accessibility of the electrolyte ions, created by the splitting, as well as the substantially straight conductive paths based on the vertically aligned structure. For the pristine VA-CNT carpet, CNTs are densely packed together, limiting the formation of an effective electrochemical double layer along their outside surfaces. Upon unzipping, the strong bundling between CNTs was weakened, as indicated by the observation of individual CNTs in Figure S1. And by opening the outermost layer of CNTs, the surfaces of the inner tubes became accessible. BET measurements of the VA-CNT carpet before and after splitting showed that the specific surface area of the material increased from 191 to 308 m^2/g. The expanded intertube spaces and more effective surface areas could facilitate the formation of an electrochemical double layer, thus enhancing the capacitance. Moreover, a three-electrode CV measurement was conducted using split VA-CNTs at a voltage rate of 20 mV/s (Figure S7), and cathodic and anodic peaks occurred at ~0.5 and 0.7 V, indicating some contribution of pseudocapacitance that may come from edges of the unzipped CNTs. In addition, in the case of partial splitting, the remaining inner tubes retain their electrical conductivity, which facilitates charge transport during the electrochemical process.

The performance of the split VA-CNT carpet electrode was also evaluated by measuring the galvanostatic discharge at different rates (Figure S6c).

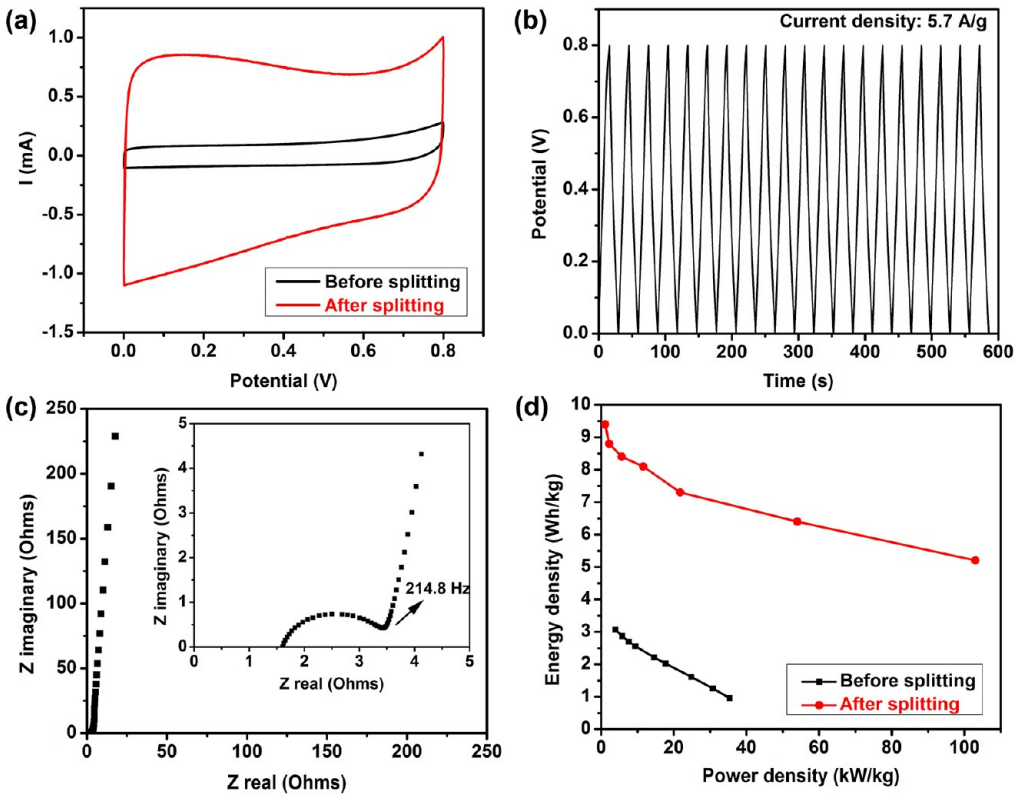

Figure 5. Measurements of supercapacitor performance. (a) Comparison of CV curves of the VA-CNT carpets before and after splitting measured at a scan rate of 0.1 V/s. (b) Galvanostatic charge–discharge curves for 20 cycles at a constant current density of 5.7 A/g of the split VA-CNT carpet electrode. (c) Nyquist plot of the split VA-CNT carpet electrode measured by amplitude current frequency scanning from 1000 kHz to 0.01 Hz. A high-frequency region of the Nyquist plot is shown in the inset with its knee frequency of 214.8 Hz. (d) A Ragone plot showing the relationship between the energy density and power density of the VA-CNT carpet supercapacitor electrode before and after splitting.

The initial IR drop can hardly be observed for our measurements, indicating that the equivalent series resistance (ESR) is rather low and the electron transfer causes little voltage limitation. The galvanostatic charge–discharge cycle measured for 20 cycles at a constant current density of 5.7 A/g of the split VA-CNT supercapacitor device is shown in Figure 5b. The near-triangular shape of each cycle suggests a capacitive behavior with almost no Faradic process. Retention of capacitance after >2000 charge–discharge cycles has also been tested, as can be seen in Figure S6c. The capacitance after 2000 cycles remained at >95% of its original value. SEM images that compare the VA-CNT carpet before and after splitting (Figure S8) also suggests that there is little obvious structural degradation during the cyclability testing.

The Nyquist plot measurement shown in Figure 5c was done at 10 mV *vs* an open circuit voltage from 1000 kHz to 0.01 Hz to determine the frequency response as well as the ESR of the supercapacitor device. There is a semicircle intersecting the real axis in the high frequency region, and the plot transforms to a vertical line with decreasing frequency, suggesting a distributed-capacitance behavior of a porous structure.[41] As can be shown, the slope is almost parallel to the imaginary axis in the low frequency region, implying that the split VA-CNT carpet electrode shows a capacitive behavior at low frequency.[42] The split VA-CNT carpet shows a high knee frequency of 214.8 Hz, as is shown in the inset in Figure 5c, which suggests that most of the stored energy is accessible even at frequencies ≥210 Hz, exhibiting a potential for applications in hybrid electrical vehicles (HEVs). This knee frequency is much larger than commercially available electrochemical supercapacitors[43] and some reported values for the MWCNT electrode[21] and VA-CNT carpet electrode,[26,27,30] which could be the result of fast electrolyte ions access and diffusion through the carpet conductive paths and the split pores.

A Ragone plot is presented in Figure 5d to interpret the maximum performance limit of the split VA-CNT electrode. The energy density and power density are calculated from galvanostatic charge–discharge curves using eqs 1 and 2:

$$E_{sp} = \frac{C_{sp}V^2}{2} \quad (1)$$

$$P_{sp} = \frac{E_{sp}}{\Delta t} \quad (2)$$

where the E_{sp} represents the energy density, P_{sp} represents the power density, C_{sp} is the specific capacitance, V is the potential after IR drop, and Δt

is the discharge time. The energy density and power density are in the range of 5.2−9.4 Wh/kg and 1.1−103 kW/kg, respectively. It can be seen that the split VA-CNT can provide a power density up to 103 kW/kg, while maintaining an energy density of ~5.2 Wh/kg. The energy density does not change appreciably with increased power density. This is higher than the reported value of energy density and power density for the current electrochemical capacitor technology[44] and VA-CNT electrode[27] and some SWCNT electrode material.[45] It is also comparable to that of VA-CNTs used in organic electrolyte[24,30] and some SWCNT electrodes.[32,33,46] As a comparison, when a pristine VA-CNT carpet was used as the active material, a maximum energy density of ~3.1 Wh/kg was measured, and the maximum power density was ~35 kW/kg at an energy density of 0.95 Wh/kg. The split VA-CNT carpet not only allows the rapid delivery of stored charges through each individual tube that is connected directly to the metallic backing plate, but also provides more effective accessibilities for the ions. The energy density might be improved by using an organic electrolyte to enlarge the potential window.

CONCLUSIONS

Splitting of VA-CNT carpets with preservation of vertical structural integrity and alignment has been realized by high-temperature potassium vapor intercalation and subsequent solution quenching. TEM analyses have shown that the split VA-CNT carpet contains GNRs and partially split MWCNTs. It is found that the partially split structures usually have split outer graphitic walls coating the outside of the inner intact few-walled nanotubes. SEM, AFM and Raman analyses confirmed the split features in the split VA-CNT carpet. Supercapacitor testing shows that the splitting treatment increased the specific capacitance by ~4 times. Furthermore, the split VA-CNT carpet electrode also exhibits stable cyclability and AC frequency response. The superior electrochemical supercapacitor performance of the split VA-CNT carpet electrode likely originates from more specific surface area due to the additional intra tube space and inner tube surface, the good conductivity of the partially split CNTs, and the vertical alignment of the conductive paths between the tubes. The investigations here show that the splitting approach is an enabling technology for generating high-performance energy conversion and storage materials.

METHODS

Synthesis of VA-CNT Carpet. The substrate for growing MWCNT carpets was prepared by electron-beam evaporating a 10 nm Al_2O_3 buffer layer and 3 nm Fe catalyst layer sequentially onto the SiO_2 wafer in an electron-beam evaporator. Vertically aligned MWCNT carpets were grown on this substrate in a hot-filament apparatus using the previously reported water-assisted chemical vapor deposition (CVD) method.[19,47] Typically, a mixture of H_2 (210 sccm), C_2H_2 (5.8 sccm) and H_2O (200 sccm) gas was flowed into the reactor at 750 °C at an elevated pressure (~25 Torr). A tungsten hot filament was activated with a current of ~9 A for 30 s to reduce the catalysts by generating atomic hydrogen in order to initiate the MWCNT nucleation. The pressure was then decreased immediately to 4.9 Torr to resume the MWCNT carpet growth. A 15-min-growth process enabled a vertical MWCNT carpet with a height of ~30 μm.

Splitting of VA-CNT Carpet. The VA-CNT carpet sample was loaded into a glass ampule along with ~50 mg potassium in a glovebox purged with N_2. The ampule was then evacuated and sealed under vacuum using an acetylene torch. The ampule was placed in a muffle furnace (NEY 6-160A) and heated at 450 °C for 48 h. During this process, the potassium vaporized and intercalated into the inner space between the walls of the MWCNTs. After cooling, the ampule was transferred into a glovebox and opened. Ethyl ether was added to the reaction mixture to protect the sample from the atmosphere; it was removed from the glovebox. Methanol was added to quench the intercalated potassium. The H_2 gas generated and the resulting volume expansion produces further splitting and exfoliation of the outer walls of MWCNTs. Finally, the split VA-CNT was washed sequentially with water and ethanol to remove byproducts before drying in a vacuum oven at 60 °C for 24 h.

Fabrication of a VA-CNT Carpet Supercapacitor and Electrochemical Measurements. The split VA-CNT carpet was immersed into a buffered oxide etch solution (buffered HF, a wet etchant to remove the SiO_2, J. T. Baker) to detach the carpet from the substrate. After ~5 min of etching, the split VA-CNT carpet film floated to the surface of the solution. Then the free-standing split VA-CNT carpet was rinsed in the DI water to remove residual acid until the rinsewater was pH neutral. The samples were rinsed in ethanol and dried in vacuum oven before assembling them into the supercapacitor device.[39,40] The split VA-CNT carpet capacitor was fabricated by sandwiching filter paper as a separator between two VA-CNT carpet sheet electrodes (Figure S5a). In one experiment, 70 μg of split VA-CNT carpet was used as active material, as weighed by a microbalance (Citizen scale, model: CM 21x, weighing accuracy 1 μg). For the control experiment, 36 μg of pristine VA-CNT carpet was used. The two electrodes were then compacted and sealed with two stainless steel plates, without using other current collectors. The effective size of the VA-CNT carpet sheet electrode was 0.2 cm^2 with a rectangular shape. The electrochemical properties were investigated using a two-electrode cell configuration with 6 M KOH as the electrolyte. Measurements were conducted with a CHI 608D potentiostat/galvanostatic for testing the cyclic voltammetry, galvnostatic charge−discharge performance and electrochemical impedance spectroscopy. No penetration of the nanotubes into the separator was observed after the two counter-electrodes were taken apart, indicating that there is likely little or no occurrence of self-discharge due to an internal short circuit.

Characterization. XPS was conducted on a PHI Quantera SXM scanning X-ray microscope. An Al anode at 25 W was used as an X-ray source with a pass-energy of 26.00 eV, 45° takeoff angle, and a 100 μm beam size. SEM images were taken at 20 kV on a FEI Quanta 400 ESEM FEG scanning electron microscope and JEOL 6500F scanning electron microscope. For TEM sample preparation, the material was dispersed in chloroform by bath-sonication using an ultrasonic cleaner (Cole-Parmer model 08849-00) for 5 min, followed by deposition on a Lacey Formvar/carbon copper grid with 300 mesh (Ted Pella, 01883-F). TEM imaging was conducted on a JEOL 2100 field emission gun transmission electron microscope. AFM images were obtained on a Digital Instrument Nanoscope IIIA atomic force microscope.

Raman spectra data was collected on an InVia Renishaw microscope using 514.5 nm argon laser. BET surface area was measured on a Quantachrome autosorb-3b BET surface analyzer.

Conflict of Interest: The authors declare no competing financial interest.

Acknowledgment. The authors acknowledge Prof. N. Zhao and Prof. J. Li at Tianjin University for helpful discussions and assistance, X. He for assisting in electron-beam evaporation, L. Li, Z. Yan and C. Xiang for helpful discussions, and the China Scholarship Council for partial support of this research. This research was funded by Lockheed Martin LANCER IV, NSF EEC-0647452, AFOSR (FA9550-09-1-0581) and the Air Force Research Laboratory (FA8650-07-2-5061).

Supporting Information Available: Further characterization data on the splitting products and the supercapacitor testing data. This material is available free of charge *via* the Internet at http://pubs.acs.org.

REFERENCES AND NOTES

1. Jorio, A.; Dresselhaus, M, D.; Dresselhaus, G. *Carbon Nanotubes: Advanced Topics in the Synthesis, Structure, Properties and Applications*; Springer-Verlag: New York, 2008; pp 13−61.
2. Han, M, Y.; Ozyilmaz, B.; Zhang, Y.; Kim, P. Energy Band-Gap Engineering of Graphene Nanoribbons. *Phys. Rev. Lett.* **2007**, *98*, 206805.
3. Li, X.; Wang, X.; Zhang, L.; Lee, S.; Dai, H. Chemically Derived, Ultrasmooth Graphene Nanoribbons Semiconductors. *Science* **2008**, *319*, 1229–1232.
4. Jiao, L.; Zhang, L.; Wang, X.; Diankov, G.; Dai, H. Narrow Graphene Nanoribbons from Carbon Nanotubes. *Nature* **2009**, *458*, 877–880.
5. Cano-Marquez, A. G.; Rodrguez-Macas, F. J.; Campos-Delgado, J.; Espinosa-Gonzalez, C. G.; Tristan-Lopez, F.; Ramrez-Gonzalez, D.; Cullen, D. A.; Smith, D. J.; Terrones, M.; Veg-Cantu, Y. I. Ex-MWNTs: Graphene Sheets and Ribbons Produced by Lithium Intercalation and Exfoliation of Carbon Nanotubes. *Nano Lett.* **2009**, *9*, 1527–1533.
6. Morelos-Gomez, A.; Vega-Daz, S, M.; Gonzalez, V, J.; Tristan-Lopez, F.; Cruz-Silva, R.; Fujisawa, F.; Muramatsu, H.; Hayashi, T.; Mi, X.; Shi, Y, F.; *et al.* Clean Nanotube Unzipping by Abrupt Thermal Expansion of Molecular Nitrogen: Graphene Nanoribbons with Atomically Smooth Edges. *ACS Nano* **2012**, *6*, 2261–2272.
7. Elias, A, L.; Botello-Mendez, A, R.; Meneses-Rodrguez, D.; Gonzalez, V, J.; Ramrez-Gonzalez, D.; Ci, L, J.; Munoz-Sandoval, E.; Ajayan, P, M.; Terrones, H.; Terrones, M. Longitudinal Cutting of Pure and Doped Carbon Nanotubes to Form Graphitic Nanoribbons using Nanoclusters as Nanoscalpels. *Nano Lett.* **2010**, *10*, 366–372.
8. Kim, K.; Sussman, A.; Zettl, A. Graphene Nano-Ribbons Obtained by Electrically Unwrapping Carbon Nanotubes. *ACS Nano* **2010**, *4*, 1362–1366.
9. Li, Y, G.; Zhou, W.; Wang, H, L.; Xie, L, M.; Liang, Y, Y.; Wei, F.; Idrobo, J.; Pennycook, S, J.; Dai, H, J. An Oxygen Reduction Electrocatalyst Based on Carbon Nanotube-Graphene Complexes. *Nat. Nanotechnol.* **2012**, *7*, 394–400.
10. Kosynkin, D. V.; Higginbotham, A. L.; Sinitskii, A.; Lomeda, J. R.; Dimiev, A.; Katherine Price, B.; Tour, J. M. Longitudinal Unzipping of Carbon Nanotubes To Form Graphene Nanoribbons. *Nature* **2009**, *458*, 872–877.
11. Kosynkin, D. V.; Lu, W.; Sinitskii, A.; Pera, G.; Sun, Z. Z.; Tour, J. M. Highly Conductive Graphene Nanoribbons by Longitudinal Splitting of Carbon Nanotubes using Potassium Vapor. *ACS Nano* **2011**, *5*, 968–974.
12. Genorio, B.; Lu, W.; Dimiev, A. M.; Zhu, Y.; Raji, A.; Novosel, B.; Alemany, L. B.; Tour, J. M. *In Situ* Intercalation Replacement and Selective Functionalization of Graphene Nanoribbon Stacks. *ACS Nano* **2012**, *6*, 4231–4240.
13. Genorio, B.; Peng, Z.; Lu, W.; Hoelscher, B. K. P.; Novosel, B.; Tour, J. M. Synthesis of Dispersible Ferromagnetic Graphene Nanoribbon Stacks with Enhanced Electrical Percolation Properties in a Magnetic Field. *ACS Nano* **2012**, *6*, 10396–10404.
14. Lu, W.; Ruan, G.; Genorio, B.; Zhu, Y.; Novosel, B.; Peng, Z.; Tour, J. M. Functionalized Graphene Nanoribbons *via* Anionic Polymerization Initiated by Alkali Metal-Intercalated Carbon Nanotubes. *ACS Nano* **2013**, *7*, 2669–2675.
15. Zhang, Z.; Sun, Z.; Yao, J.; Kosynkin, D. V.; Tour, J. M. Transforming Carbon Nanotube Devices into Nanoribbons Devices. *J. Am. Chem. Soc.* **2009**, *131*, 13460–13463.
16. Jiao, L, Y.; Zhang, L.; Ding, L.; Liu, J.; Dai, H, J. Aligned Graphene Nanoribbons and Crossbars from Unzipped Carbon Nanotubes. *Nano Res.* **2010**, *3*, 387–394.
17. Pint, C, L.; Nicholas, N, W.; Xu, S.; Sun, Z.; Tour, J, M.; Schmidt, H, K.; Gordon, R, G.; Hauge, R, H. Three Dimensional Solid-State Supercapacitors from Aligned Single-Walled Carbon Nanotube Array Templates. *Carbon* **2011**, *49*, 4890–4897.
18. Giubileo, F.; Di Bartolomeo, A.; Scarfato, A.; Iemmo, L.; Bobba, F.; Passacantando, M.; Santucci, S.; Cucolo, A. M. Local Probing of the Field Emission Stability of Vertically Aligned Multi-Walled Carbon Nanotubes. *Carbon* **2009**, *47*, 1074–1080.
19. Pint, C. L.; Xu, Y. Q.; Pasquali, M.; Hauge, R. H. Formation of Highly Dense Aligned Ribbons and Transparent Films of Single-Walled Carbon Nanotubes Directly from Carpets. *ACS Nano* **2008**, *2*, 1871–1878.
20. Gonzalez-Carretero, J.; Castillo-Martinez, E.; Dias-Lima, M.; Acik, M.; Rogers, D. M.; Sovich, J.; Haines, C. S.; Lepro, X.; Kozlov, M.; Zhakidov, A.; *et al.* Oriented Graphene Nanoribbon Yarn and Sheet from Aligned Multi-Walled Carbon Nanotube Sheets. *Adv. Mater.* **2012**, *24*, 5695–5701.
21. Gogosti, Y.; Simon, P. True Performance Metrics in Electrochemical Energy Storage. *Science* **2011**, *334*, 917–918.
22. Miller, J. R.; Simon, P. Electrochemical Capacitors for Energy Management. *Science* **2008**, *321*, 651–652.
23. Niu, C. M.; Sichel, E. K.; Hoch, R.; Moy, D.; Tennent, H. High Power Electrochemical Capacitors Based on Carbon Nanotube Electrodes. *Appl. Phys. Lett.* **1997**, *70*, 1480–1482.
24. Kim, B.; Chung, H.; Kim, W. High-Performance Supercapacitors Based on Vertically Aligned Carbon Nanotubes and Nonaqueous Electrolytes. *Nanotechnology* **2012**, *23*, 155401.
25. Yoon, B. J.; Jeong, S. H.; Lee, K. H.; Kim, H. S.; Park, C. G.; Han, J. H. Electrical Properties of Electrical Double Layer Capacitors with Integrated Carbon Nanotube Electrodes. *Chem. Phys. Lett.* **2004**, *388*, 170–174.
26. Shah, R.; Zhang, X. F.; Talapatra, S. Electrochemical Double Layer Capacitor Electrodes using Aligned Carbon Nanotubes Grown Directly on Metals. *Nanotechnology* **2009**, *20*, 395202.
27. Zhang, H.; Cao, G. P.; Wang, Z. Y.; Yang, Y. S.; Gu, Z. N. Electrochemical Capacitive Properties of Carbon Nanotube Arrays Directly Grown on Glassy Carbon and Tantalum Foils. *Carbon* **2008**, *46*, 822–824.
28. Gao, L. J.; Peng, A. P.; Wang, Z. Y.; Zhang, H.; Shi, Z. J.; Gu, Z. N.; Cao, G. P.; Ding, B. Z. Growth of Aligned Carbon Nanotube Arrays on Metallic Substrate and Its Application to Supercapacitors. *Solid State Commun.* **2008**, *146*, 380–383.
29. Honda, Y.; Haramoto, T.; Takeshige, M.; Shiozaki, H.; Kitamura, T.; Ishikawa, M. Aligned MWCNT Sheet Electrodes Prepared by Transfer Methodology Providing High-Power Capacitor Performance. *Electrochem. Solid State Lett.* **2007**, *10*, A106–A110.
30. Lu, W.; Qu, L. T.; Henry, K.; Dai, L. M. High Performance Electrochemical Capacitors from Aligned Carbon Nanotube Electrodes and Ionic Liquid Electrolytes. *J. Power Sources* **2009**, *189*, 1270–1277.
31. Ci, L. J.; Manikoth, S. H.; Li, X. S.; Vajtai, R.; Ajayan, P. M. Ultrathick Freestanding Aligned Carbon Nanotube Films. *Adv. Mater.* **2007**, *19*, 3300–3303.
32. Izadi-Najafabadi, A.; Yasuda, S.; Kobashi, K.; Yamada, T.; Futaba, D, N.; Hatori, H.; Yumura, M.; Iijima, S.; Hata, K. Extracting the Full Potential of Single-Walled Carbon Nanotubes as Durable Supercapacitor Electrodes Operable at 4 V with High Power and Energy Density. *Adv. Energy Mater.* **2010**, *22*, E235–E241.

33. Futaba, D. N.; Hata, K. J.; Yamada, T.; Hiraoka, T.; Hayamizu, Y.; Kakudate, Y.; Tanaike, O.; Hatori, H.; Yumura, M.; Iijima, S. Shape-Engineerable and Highly Densely Packed Single-Walled Carbon Nanotubes and Their Application as Super-Capacitor Electrodes. *Nat. Mater.* **2006**, *5*, 987–994.
34. Suzuki, S.; Bower, C.; Zhou, O. *In Situ* TEM and EELS Studies of Alkali-Metal Intercalation with Single-Walled Carbon Nanotubes. *Chem. Phys. Lett.* **1998**, *285*, 230–234.
35. Lee, R. S.; Kim, H. J.; Fischer, J. E.; Thess, A.; Smalley, R. E. Conductivity Enhancement in Single-Walled Carbon Nanotube Bundles Doped with K and Br. *Nature* **1997**, *388*, 255–257.
36. Miyata, Y.; Suzuki, M.; Fujihara, M.; Asada, Y.; Kitaura, R.; Shinohara, H. Solution-Phase Extraction of Ultrathin Inner Shells from Double-Wall Carbon Nanotubes. *ACS Nano* **2010**, *4*, 5807–5812.
37. Viculis, L. M.; Mack, J. J.; Kaner, R. B. A Chemical Route to Carbon Nanoscrolls. *Science* **2003**, *299*, 1361.
38. Ferrari, A. C.; Robertson, J. Interpretation of Raman Spectra of Disordered and Amorphous Carbon. *Carbon* **2000**, *61*, 14095–14107.
39. Zhu, Y.; Li, L.; Zhang, C.; Casillas, G.; Sun, Z.; Yan, Z.; Ruan, G.; Peng, Z.; Raji, A. O.; Kittrell, C.; *et al.* A Seamless Three-Dimensional Carbon Nanotube Graphene Hybrid Material. *Nat. Commun.* **2012**, *3*, 1225.
40. Lin, J.; Zhang, C.; Yang, Z.; Zhu, Y.; Peng, Z.; Hauge, R. H.; Natelson, D.; Tour, J. M. 3-Dimensional Graphene Carbon Nanotube Carpet-Based Microsuper Capacitors with High Electrochemical Performance. *Nano Lett.* **2013**, *13*, 72–78.
41. Nian, Y. R.; Teng, H. Influence of Surface Oxides on the Impedance Behavior of Carbon-Based Electrochemical Capacitors. *J. Electroanal. Chem.* **2003**, *540*, 119–127.
42. Taberna, P. L.; Simon, P.; Fauvarque, J. F. Electrochemical Characteristics and Impedance Spectroscopy Studies of Carbon-Carbon supercapacitors. *J. Electrochem. Soc.* **2003**, *150*, A292–A300.
43. Miller, J. R. Battery-Capacitor Power Source for Digital Communication: Simulations Using Advanced Electrochemical Capacitors. *Proc. Electrochem. Soc.* **1996**, *95−29*, 246–254.
44. Burke, A.; Arulepp, M. Recent Developments in Carbon-Based Electrochemical Capacitors: Status of the Technology and Future Prospects. *Proc. Electrochem. Soc.* **2003**, *2001−21*, 576–591.
45. Chen, J. H.; Li, W. Z.; Wang, D. Z.; Yang, S. X.; Wen, J. G.; Ren, Z. F. Electrochemical Characterization of Carbon Nanotubes as Electrode in Electrochemical Double-Layer capacitors. *Carbon* **2002**, *40*, 1193–1197.
46. Niu, Z.; Zhou, W.; Chen, J.; Feng, G.; Li, H.; Ma, W.; Li, J.; Dong, H.; Ren, Y.; Zhao, D.; *et al.* Compact-Designed Supercapacitors using Free-Standing Single-Wall Carbon Nanotube Films. *Energy Environ. Sci.* **2011**, *4*, 1440–1446.
47. Zhang, C. G.; Bets, K.; Lee, S. S.; Sun, Z.; Mirri, F.; Colvin, V. L.; Yakobson, B. I.; Tour, J. M.; Hauge, R. H. Closed-Edged Graphene Nanoribbons from Large Diameter Collapsed Nanotubes. *ACS Nano* **2012**, *6*, 6023–6032.